Cellular and Molecular Neurobiology (2019) 39:857–869
https://doi.org/10.1007/s10571-019-00685-5

ORIGINAL RESEARCH

Hydrogen Alleviates Necroptosis and Cognitive Deficits in Lithium–Pilocarpine Model of Status Epilepticus

Ruihua Jia[1,2] · Ning Jia[2,3] · Fang Yang[1] · Zihe Liu[2] · Rui Li[2] · Yongli Jiang[1] · Jingjing Zhao[1] · Lu Wang[3] · Shuo Zhang[4] · Zhengping Zhang[5] · Haifeng Zhang[2] · Shengxi Wu[2] · Fang Gao[2] · Wen Jiang[1]

Received: 17 February 2019 / Accepted: 7 May 2019 / Published online: 14 May 2019

Abstract

Status epilepticus without prompt seizure control always leads to neuronal death and long-term cognitive deficits, but effective intervention is still absent. Here, we found that hydrogen could alleviate the hippocampus-dependent spatial learning and memory deficit in lithium–pilocarpine model of status epilepticus in rats, as evidenced by the results in Morris water maze test. Hydrogen treatment downregulated the expression of necroptosis-related proteins, such as MLKL, phosphorylated-MLKL, and RIPK3 in hippocampus, and further protected neurons and astrocytes from necroptosis which was here first verified to occur in status epilepticus. Hydrogen also protected cells from apoptosis, which was indicated by the decreased cleaved-Caspase 3 expression. Meanwhile, Iba1$^+$ microglial activation by status epilepticus was reduced by hydrogen treatment. These findings confirm the utility of hydrogen treatment in averting cell death including necroptosis and alleviating cognitive deficits caused by status epilepticus. Therefore, hydrogen may provide a potential and powerful clinical treatment for status epilepticus-related cognitive deficits.

Keywords Status epilepticus · Hydrogen · Necroptosis · Apoptosis · Cognitive deficit

Introduction

Status epilepticus (SE) is a severe medical emergency with high mortality and morbidity (Betjemann and Lowenstein 2015; Seinfeld et al. 2016). It was reported that continuous seizure activity in SE is an increased risk for cognitive deficits both in animal models and in clinical patients (Auvin et al. 2016). Pathological observation revealed that persistent and repeated abnormal discharges in SE could induce the generation of reactive oxygen species, which in turn leads to the death of neurons (Pearson et al. 2015; Walker 2018). In severe cases, the deteriorated cell destruction even lead to fibrosis of the hippocampus such as in temporal lobe epilepsy which is the most common type of epilepsy in adults (Sharma et al. 2007; Schauwecker 2012; Levesque et al. 2016). Multiple downstream mechanisms including inflammation and other changes followed cell death closely (Auvin et al. 2016; Walker 2018). All these pathological changes, including cell death, cell death-caused structural abnormity, and inflammation processes, contribute to the cognitive decline consequences. On clinical trials, the safety and efficacy of different treatment strategies have been tested (Haut et al. 2016; Trinka et al. 2015, 2016). Benzodiazepines

Ruihua Jia, Ning Jia, and Fang Yang are Co-first authors.

Electronic supplementary material The online version of this article (https://doi.org/10.1007/s10571-019-00685-5) contains supplementary material, which is available to authorized users.

✉ Fang Gao
gao_fang_2011@163.com

✉ Wen Jiang
jiangwen@fmmu.edu.cn

1 Department of Neurology, Xijing Hospital, Fourth Military Medical University, 127 Chang Le Xi Road, Xi'an 710032, Shaanxi, China

2 Department of Neurobiology and Institute of Neurosciences, School of Basic Medicine, Fourth Military Medical University, 169 Chang Le Xi Road, Xi'an 710032, Shaanxi, China

3 The Medical College of Yan'an University, 19 Guanghua Street, Yan'an 716000, Shaanxi, China

4 Department of Diagnostic Radiology, First Affiliated Hospital of Xi'an Jiaotong University, 277 West Yanta Road, Xi'an 710061, Shaanxi, China

5 Hong Hui Hospital, Xi'an Jiaotong University College of Medicine, 555 Youyi Road, Xi'an 710054, Shaanxi, China

(BZDs), considered as first-line options among early treatments, can effectively control status promptly and thus protect permanent and progressive cognitive function deficit caused by ongoing seizures in brain, but they are only able to control SE in about two-thirds of all patients (Seinfeld et al. 2016; Trinka et al. 2015, 2016; Trinka and Kalviainen 2017). Therefore, researchers are still striving to find novel strategies to relieve the cognitive deficits in patients.

It has been shown that hydrogen could effectively protect the survival of neurons through reducing cytotoxic reactive oxygen radicals in cerebral ischemia, which finally ameliorated brain injury (Ohsawa et al. 2007; Cai et al. 2009). Hydrogen treatment was applied for other types of diseases such as subarachnoid hemorrhage-related brain injury, carbon monoxide poisoning, postoperative ileus, ovarian ischemia reperfusion (Sun et al. 2011; Wang et al. 2013; Okamoto et al. 2016; Shao et al. 2016; Gokalp et al. 2017). So we suppose hydrogen may promote the neural function in SE, which has not been reported before. To address this question, we delivered hydrogen-rich saline (HRS) intraperitoneally (Shao et al. 2016) in lithium–pilocarpine (Li-Pilo)-induced SE rat model which resembles many features of human temporal lobe epilepsy including cognitive deficits (Curia et al. 2008; Levesque et al. 2016). Through behavior test, Western Blot (WB) analysis, immunofluorescence staining, and transmission electron microscopy, we found that hydrogen partially restored the hippocampus-dependent brain function affected by SE, including spatial learning and memory in water mazes. Hydrogen reduced neuronal apoptosis induced by SE. More importantly, we found that neurons in CA1 were also vulnerable to necroptosis in SE rat model, and hydrogen treatment reduced the neural cell necroptosis. Also, local microglial activation in hippocampus was reduced by hydrogen treatment. Finally, these effects may contribute to the final cognitive improvement by hydrogen.

Materials and Methods

Lithium–Pilocarpine-Induced SE Models

Male Sprague–Dawley rats weighing about 200 g were selected and intraperitoneally injected with lithium chloride (180 mg/kg, Sigma, SLBP9949 V). 18–20 h later, pilocarpine (30 mg/kg, Sigma, 14487-5) was administrated to each rat by intraperitoneal injection. The degree of seizure was assessed, and the rats were treated with diazepam (10 mg/kg, Kingyork Group, 2744) after they reached SE for 10 min. Rats of the experimental SE group were sequentially given diazepam and HRS (20 ml/kg) with 5-min interval through intraperitoneal injection (Cai et al. 2009; Sun et al. 2011; Wang et al. 2013; Ohta 2014; Iida et al. 2016; Shao et al. 2016). Those of the control SE group were given diazepam with saline (20 ml/kg). For the blank control group, normal rats without lithium–pilocarpine administration were delivered saline or HRS with the same concentration at consistent time points. HRS refers to the saline in which hydrogen was saturated.

All rats were maintained in specific pathogen-free conditions with access to food and water freely. The room for rats was controlled at 20–22 °C with a 12-h light/12-h dark cycle. All animal experiments were carried out in accordance with the National Institutes of Health (NIH) guidelines for the use of experimental animals, and approved by the Animal Experiment Administration Committee of the Fourth Military Medical University.

Immunofluorescence Staining

Three days after SE modeling and/or HRS treatment, animals were anesthetized with 2% pentobarbital (100 mg/kg), followed by perfusion fixation of brain tissues with 4% paraformaldehyde to make frozen (25 μm). Brain sections were washed in 0.01 M PBS (phosphate buffer solution, 10 min for three times). The primary antibodies were added, respectively, and incubated at 4 °C overnight. The primary antibodies included cleaved Caspase 3 (GeneTex, GTX22302, 1:100), MLKL (Millipore, 2894940, 1:300), NeuN (Millipore, NG1876252, 1:300), GFAP (Sigma, 023M4765, 1:1500), and Iba-1 (Wako, CTF4377, 1:1000). After the incubation of primary antibody and being re-washed in PBS, the secondary antibodies were incubated at room temperature for 2 h. Brain sections were then washed again and followed by Hoechst (Solarbio, B8030, 1:2000) staining (room temperature for 20 min). Finally, the sections were mounted with glycerol in PBS. Images were acquired using Olympus FV1000 confocal microscope.

Transmission Electron Microscopy

The animals were anesthetized and perfused with a mixed solution of 4% paraformaldehyde and 2% glutaraldehyde, followed by post-fixation with a 4% glutaraldehyde solution for 2 h. Brain tissues were cut on a vibratome (Leica, VT1000 s) at 100 μm, washed 5 times with 0.1 M PB (Phosphate Buffer, 6 min per time), and fixed by 1% osmic acid for 2 h. Then, slices were washed with 0.1 M PB for another 5 times to remove osmic acid. Gradient dehydration by ethyl alcohol (50%, 70%, 80%, 85%, 95%) was performed (each for 10 min), followed by washing with absolute ethanol and acetone (both 5 min with three times). The slices were then immersed in a 1:1 mixture of acetone and embedding agent (SPI-PON 812, Structure Probe, Inc, 02660-AB) at 37 °C for 2 h, followed by being tablet embedded with pure embedding agent overnight.

The tablet was subjected to film positioning, and the target region was selected and then subjected to ultrathin sectioning (80–90 nm). Sections were stained with lead and uranium for 5 min each and then observed with transmission electron microscope.

Western Blot

After the extraction of hippocampus, tissues were lysed in RIPA buffer (Beyotime, P0013C) containing 1% protease inhibitor and phosphatase inhibitor (Beyotime, P1005 and P1045). Equal amounts of protein samples were electrophoresed using SDS–polyacrylamide gels and transferred to PVDF membranes (Millipore, ISEQ 00010). The membranes were then blocked for 1 h and incubated with appropriate primary antibodies (Caspase 3, Novus Biologicals, NB100-56708, 1:200; MLKL, Millipore, 2894940, 1:500; p-MLKL, Abcam, ab196436, 1:500; RIPK3, Enzo, ADI-905-242-100, 1:500; GAPDH, CoWin Biosciences, CW0100 M, 1:2000) overnight at 4 °C followed by incubation of secondary antibodies (Goat Anti-Rabbit IgG, CoWin Biosciences, CW0103S; Goat Anti-Mouse IgG, CoWin Biosciences, CW0102S) for 2 h at room temperature. The bound antibodies were detected using Immobilon® Western chemiluminescence solution (Beyotime, P0018 M). Band intensities were quantified by ImageJ software. Caspase 3, MLKL, p-MLKL, and RIPK3 band intensities were normalized to GAPDH as a loading control.

Morris Water Maze

Morris Water Maze (MWM) testing was conducted in a round black pool 160 cm in diameter and water of 25 ± 0.5 °C was filled to 30 cm deep. A transparent Plexiglas platform (29 cm in height and 10 cm in diameter) was placed in the center of quadrant 1 (the target quadrant). Rats were randomly put in one of the four quadrants in the water, facing the wall of the pool. During the learning trials, if the rat failed to find the platform within 60 s, it was then gently guided to the platform and allowed to stay on the platform for 20 s. Each rat was trained 4 times a day with a 20-min interval between trials for continuous 4-day training. The distance traveled and escape latency to the platform were calculated by averaging the four trial values as indices representing the learning performance. Spatial memory was evaluated by the probe trial on day 5. The platform was removed and animals were randomly placed into the quadrants outside the original platform quadrant. The time spent in the target quadrant and the frequencies of entering the target quadrant for each rat were collected and analyzed.

Statistical Analysis

The statistical analysis was performed using GraphPad Prism 7. Repeated measures two-way ANOVA was used to compare differences in measures in the treatment groups and time points, with the interactions between factors tested when necessary. One-way ANOVA was used to test for differences among the treatment groups on the separate days in the spatial probe test. One-way ANOVA was also used to test for staining differences among groups more than two. Data from two groups were compared using Student's *t* test. For all analyses, $P < 0.05$ was considered statistically significant.

Results

Hydrogen Significantly Restored the Hippocampus-Dependent Spatial Learning and Memory Ability Impaired by SE

To determine spatial learning and memory function, rats with or without SE model were treated with HRS or vehicle, and were tested by MWM at day 14 after SE. The degree of seizure exhibited no significant difference among different groups (data not shown), and the path lengths on the first training day showed no difference (Supplementary Fig. 1a), indicating that rats of all groups have similar motor capabilities. Escape latency to reach the submerged platform was recorded to monitor the spatial learning ability. As shown in Fig. 1a, there was a reduction in escape latency across all groups as training day progressed (F (3, 12) = 20.93, $P < 0.0001$) and different treatments had different effects on escape latency (F (3, 12) = 26.49, $P < 0.0001$), although no significant interaction effect (group*days) during training days (P for interaction = 0.2220) was shown by repeated measures two-way ANOVA test. There was no significant difference in the latency between control group and HRS-treated control group (F (1, 4) = 0.0004027, $P = 0.9850$). SE significantly affected latency to find the submerged platform using spatial cues (F (1, 4) = 50.33, $P = 0.0021$). However, HRS treatment significantly restored the latency as the training proceeded (F (2, 8) = 43.49, $P < 0.0001$) (Fig. 1a). After training, a probe trial for spatial memory was conducted by removing the platform. The amount of time spent searching the target quadrant and the frequency of entering the target quadrant were counted to evaluate the memory. Significant differences were detected between saline-treated SE group and saline-treated control group in both time (Fig. 1b, $P = 0.0038$) and frequency of entering (Fig. 1c, $P = 0.0019$), suggesting that SE affected spatial memory in this task. There were no differences in these two parameters between HRS-treated control rats and saline-treated control rats (Fig. 1b, $P = 0.5774$ for amount of time,

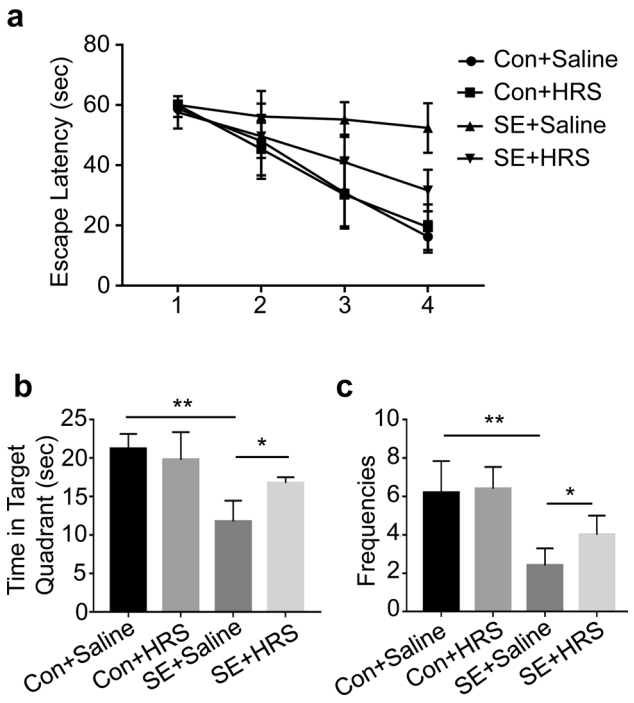

Fig. 1 HRS improved SE-induced cognitive dysfunction in spatial learning and memory. **a** Spatial learning and memory abilities were assessed by Morris Water Maze. The test showed that the escape latency to find the submerged platform by different groups all gradually decreased although to different degrees as the training progressed ($F(3, 12) = 20.93$, $P < 0.0001$). More importantly, the escape latency varied among different groups ($F(3, 12) = 26.49$). **b**, **c** After training for four days, a probe test for spatial memory was conducted on the fifth day. The amount of time spent searching the target quadrant (**b**) and the frequencies of entering the target quadrant (**c**) were recorded and compared between different groups. Data were presented as mean ± SEM and $n = 5$ in all groups. Asterisk (*) denoted a significant difference ($P < 0.05$) between groups and double asterisk (**) meant $P < 0.01$. Abbreviations in pictures were as follows. *Con* control, *sec* seconds, *SE* status epilepticus, *HRS* hydrogen-rich saline

Fig. 1c, $P = 0.8287$ for frequency). But both the total time and frequency increased in HRS-treated SE rats compared to saline-treated SE rats (Fig. 1b, $P = 0.012$ for amount of time, Fig. 1c, $P = 0.0285$ for frequency), which showed that hydrogen ameliorated the spatial memory impairment in SE rats, but did not affect the ability in normal rats. The real-time tracking showed same result (Supplementary Fig. 1b), and time spent in each quadrant was also measured (Supplementary Fig. 1c). These data suggest that the cognitive deficits in spatial learning and memory caused by SE could notably be restored by hydrogen.

SE-Induced Apoptosis in CA1 Neurons was Reduced by Hydrogen Treatment

In order to explain the therapeutic effect of hydrogen, we tested the apoptosis in hippocampus 72 h after SE. Compared to control, hippocampus in SE rats showed an increase in the expression of cleaved Caspase 3 in hippocampus (Supplementary Fig. 2a). To analyze different sub-regions, CA1 (Fig. 2), CA3 (Supplementary Fig. 2), and dentate gyrus (DG) (Supplementary Fig. 2) were observed, respectively. In CA1, SE led to a prominent increase in apoptosis as indicated by higher expression of cleaved Caspase 3 in staining (Fig. 2a, b) and WB (Fig. 2c, d) tests. HRS reduced cleaved Caspase 3^+ cells in CA1 total cells from $17.27 \pm 0.70\%$ in SE rats to $7.61 \pm 0.57\%$ in HRS-treated SE rats (Fig. 2a, b), and decreased the expression of cleaved Caspase 3 protein despite unaffected expression of total Caspase 3 (Fig. 2c, d).

To distinguish the apoptosis in neurons and astrocytes separately in CA1, cleaved Caspase 3 was double-stained with NeuN (Fig. 3a, b) or GFAP (Fig. 3c, d). As indicated in Fig. 3b, SE caused an extensive loss of neurons. HRS, however, restores the neuronal amount from $11.17 \pm 0.22\%$ in CA1 total cells to $16.37 \pm 0.43\%$, and reduced the amount of cleaved Caspase 3^+ cells in $NeuN^+$ neurons from $15.27 \pm 1.46\%$ in SE group to $9.45 \pm 0.62\%$ in HRS-treated SE group (Fig. 3b). Accordingly, the cellular structure was improved when comparing HRS-treated SE CA1 with saline-treated SE CA1 (Fig. 3a). On the contrary, HRS did not show the protective effect on astrocytes in CA1 region (Fig. 3c, d).

In CA3, HRS had no obvious effect on apoptosis (Supplementary Fig. 2b, c). In DG, HRS reduced the percentage of cleaved Caspase 3^+ cells in total cells (Supplementary Fig. 2d, e), in $NeuN^+$ neurons (Supplementary Fig. 2f, g), and in $GFAP^+$ astrocytes (Supplementary Fig. 2h, i), but it did not influence the number of neurons (Supplementary Fig. 2g) or the number of astrocytes (Supplementary Fig. 2i).

Therefore, HRS showed a protective effect to prevent cellular apoptosis in hippocampus.

Necroptosis Occurred in SE Rats with a Positional and Cellular Preference

Recent years, necroptosis as a new form of cell death was reported to be involved in many neurological diseases, such as stroke (Yang et al. 2018), spinal cord injury (Fan et al. 2016), and neurodegenerative diseases (Zhang et al. 2017). To observe necroptosis in SE and to further explain hydrogen's therapeutic effect, we next focused on necroptosis.

First, we observed necroptosis in hippocampus of SE rats by the staining of MLKL (a marker of necroptosis and an essential component of necroptosis pathway). The results about time course in SE rats (Supplementary Fig. 3) showed that MLKL expression in CA1 increased over time till 72 h after SE, and at that time the difference between SE and control group was prominent with high MLKL expression in SE hippocampus and almost absent expression in control ones (Fig. 4a). Details were assayed in different sub-regions

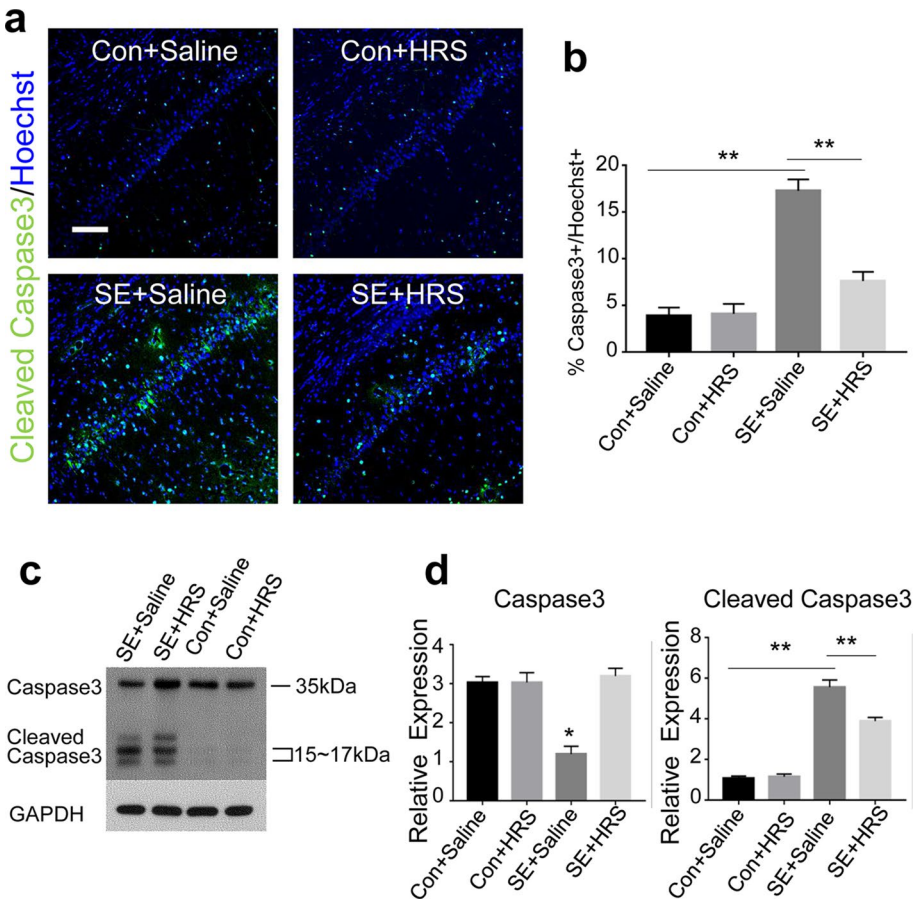

Fig. 2 The effects of HRS on apoptosis in CA1 of hippocampus. **a** Apoptosis in hippocampus was assessed by immunofluorescence staining of cleaved Caspase 3. Representative images of CA1 from each group were present. **b** Statistical results showed that the percentage of Caspase 3^+ cells in Hoechst$^+$ total cell of each field was significantly increased in SE rats compared to control ones and decreased after HRS application ($n=3$ in each group, $P<0.05$). **c**, **d** The proteins of CA1 from each group were extracted and analyzed by Caspase 3 antibody. Statistical analysis was performed. Data were presented as mean ± SEM. $^*P<0.05$; $^{**}P<0.01$. Scale bar: 100 μm

(Fig. 4b). In CA1 area, the expression of MLKL increased dramatically in SE rats compared to control ones (Fig. 4b). Statistics analysis (Fig. 4b) indicated that the percentage of MLKL$^+$ cells significantly increased from 2.3 ± 0.35% in control rats to 13.3 ± 2.23% in SE rats. In hilus of DG, SE rats also showed an obviously higher MLKL expression, from 0.73 ± 0.23 to 19.8 ± 2.60% (Fig. 4b). However in CA3, necroptosis was absent in both control and SE group (Fig. 4b). These results suggest that necroptosis contributes to cell death in CA1 and hilus of DG, but not to that in CA3.

To further confirm the occurrence of necroptosis, WB analysis and transmission electron microscopy (TEM) observation were performed in SE hippocampus. Analysis of the protein from CA1 by WB (Fig. 4c) confirmed that the expression of MLKL in SE group indeed significantly increased as compared to control groups, and more importantly, the expression of phosphorylated-MLKL (p-MLKL, a marker of activation of necroptosis pathway) increased. The expression of the interacting RIPK3 protein (an important component of necroptosis pathway) (Fig. 4c) also significantly increased in the SE group. All these results indicated the activation of necroptosis pathway after SE. CA1 neurons were further observed by TEM. The ultrastructure in Fig. 4d (8000×) demonstrated a neuron that exhibited a deformed nucleus with condensed chromatin, large vacant spaces in the cytoplasm, and swelling mitochondrial (enlarged and labeled with asterisk in Fig. 4e) which were considered to be typical features of necroptosis (Cai et al. 2017; Weinlich et al. 2017). These results robustly confirmed that necroptosis occurred in hippocampus at 72 h after SE, and that cells in some areas were vulnerable to necroptosis, including CA1 and hilus of DG.

To clarify the cell types of necroptosis in SE rats, cell type markers were co-stained with MLKL. In CA1 (Fig. 5a), NeuN$^+$ neurons in control rats lined up in order and did not show MLKL$^+$ staining while in SE ones NeuN$^+$ neurons lost the normal organized structure and some of them were double-labeled with MLKL as indicated by arrows. GFAP$^+$ astrocytes in CA1 were also tested with MLKL (Fig. 5b). The architecture of astrocytes in SE rats was not affected as compared to control and a small number of the GFAP$^+$ astrocytes were also double-labeled with MLKL (Fig. 5b). To validate the contributions to the total necroptosis in CA1 by neurons and astrocytes separately, we quantified the ration of NeuN$^+$-MLKL$^+$ cells and GFAP$^+$-MLKL$^+$ cells in MLKL$^+$ cells. The results (Fig. 5c) showed that among the total MLKL$^+$ cells in CA1, neurons accounted for 77.51 ± 1.52% and astrocytes accounted for 15.3 ± 1.26%. The MLKL$^+$ cells in hilus of DG were also

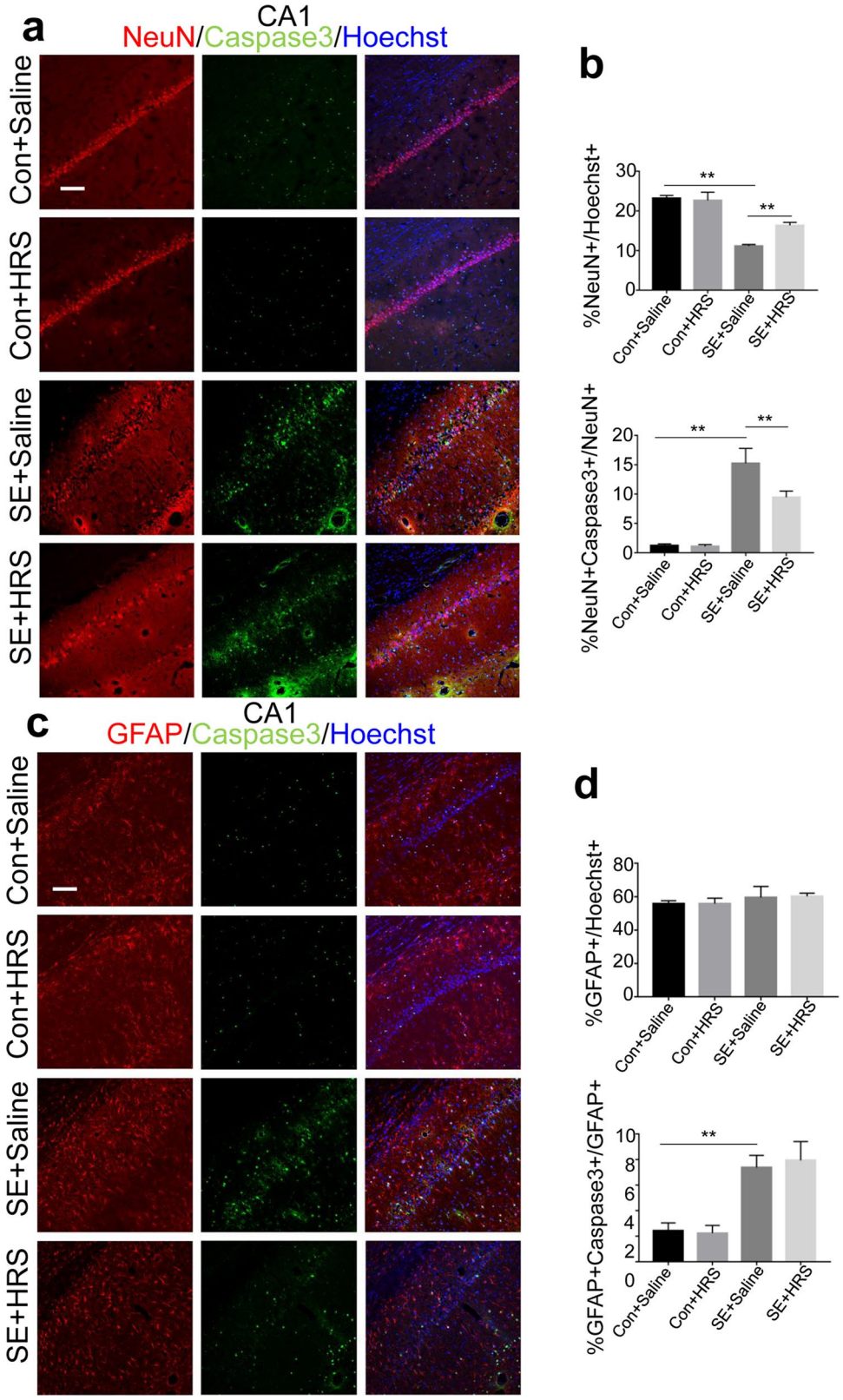

Fig. 3 Detailed effects of HRS on apoptosis in CA1 neurons and astrocytes, respectively. **a** Apoptosis in CA1 neurons were assessed by immunofluorescence staining of cleaved Caspase 3 with NeuN together ($n=3$ in each group). **b** Statistical analysis included the percentage of Caspase 3^+ neurons in total neurons of one field and the number of neurons in one field as a reflection of the protective effect. **c** Apoptosis in CA1 astrocytes was assessed by immunofluorescence staining of cleaved Caspase 3 with GFAP together ($n=3$ in each group). **d** Similar statistical analysis was performed. Data were presented as mean ± SEM. ** $P<0.01$. Scale bar: 100 μm

analyzed (Fig. 5d, e). The double-stainings were quantified and the results showed that MLKL expression in SE rats only co-expressed with GFAP (Fig. 5e, f) but not with NeuN (Fig. 5d, f). To compare the composition of cell types between apoptosis and necroptosis, we also analyzed apoptosis in Fig. 3a, c and Supplementary Fig. 2f, h. The statistical results displayed in

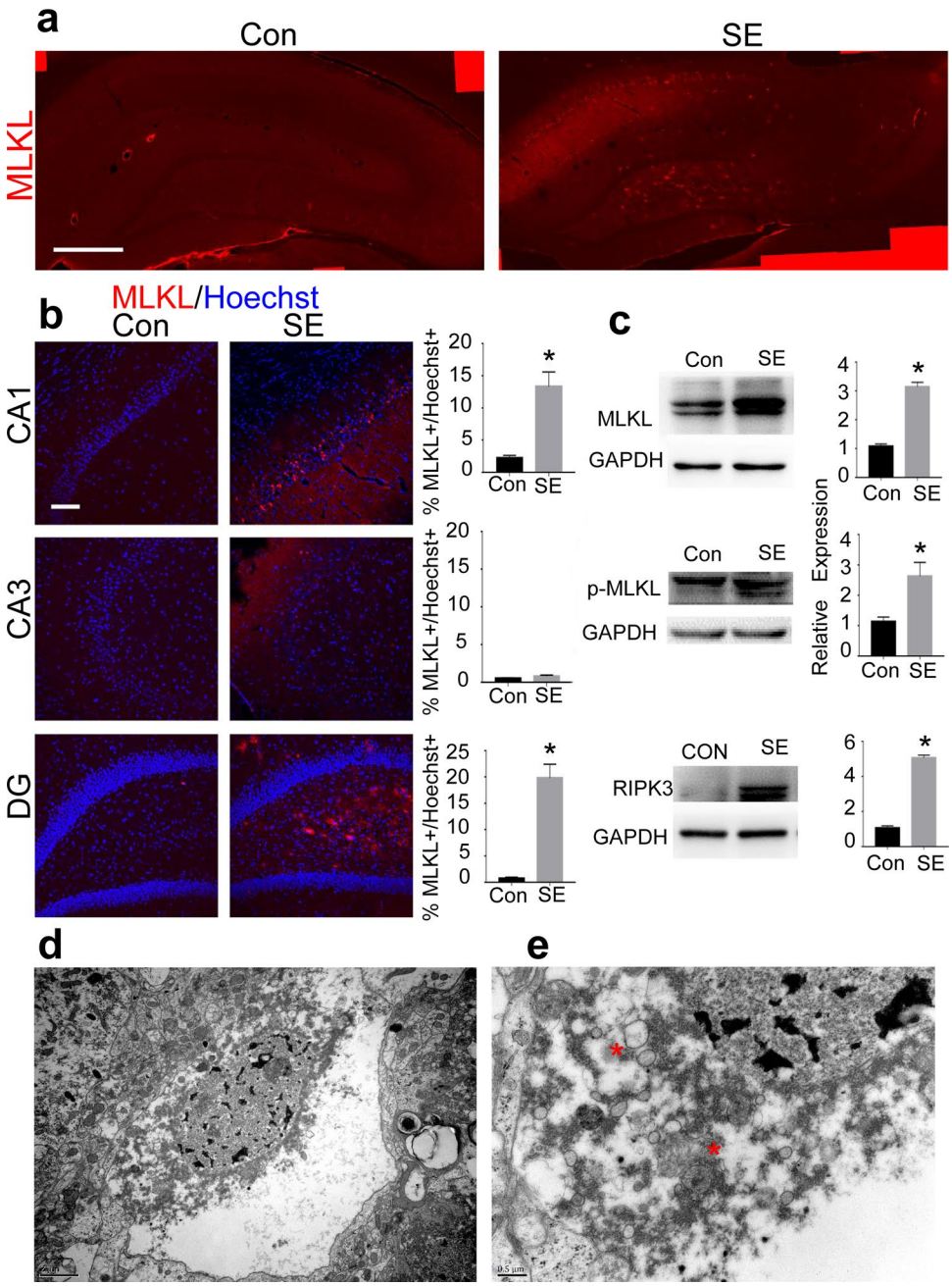

Fig. 4 SE induced necroptosis in CA1 and hilus of DG in experimental rats. **a** Hippocampus of rats from control and SE groups were analyzed by immunofluorescence staining of MLKL ($n=3$ in each group). **b** The stainings of MLKL in CA1, CA3, and DG were enlarged and representative images from both groups were presented. The proportions of $MLKL^+$ cells within the $Hoechst^+$ total cells in one field were statistically analyzed. **c** The expressions of necroptosis-related proteins in CA1 of different groups were tested by WB. The expressions of MLKL, p-MLKL, and RIP3 were significantly increased after SE ($P<0.05$). **d, e** The ultrastructure of CA1 in SE rats was observed by TEM. A representative neuron in **d** exhibited vacant spaces in the cytoplasm, loss of ribosomes, and a deformed nucleus with condensed and marginated chromatin (8000×). Part of this neuron was amplified in **e** (25000×) and the mitochondrial swelling was indicated by asterisk in the picture. Data were presented as mean ± SEM. *In **b** and **c** indicated that $P<0.05$. Scale bar: 500 μm in (**a**), 100 μm in (**b**)

Fig. 5g, h showed that apoptotic cells in CA1 and DG included both neurons and astrocytes, which presented no preference for specific type of cells. In summary, these results verified that SE could induce mainly neuronal necroptosis in CA1 and astrocytic necroptosis in hilus of DG.

Hydrogen Could Protect Cells from SE-Induced Death, Especially Protecting Neurons in CA1 from Necroptosis

We further tested the effect of hydrogen on necroptosis. The analysis of CA1 protein showed the expressions of MLKL (Fig. 6a, b), p-MLKL (Fig. 6c, d), and RIPK3 (Fig. 6e, f) were not changed in HRS-treated control group but increased significantly in SE group when compared to control one. However, these necroptosis-related proteins were dramatically decreased after HRS administration in SE group. Immunostaining (Fig. 6g–i) further strengthened this result. According to the stainings (Fig. 6g), the proportions of $MLKL^+$ cells in total cells were 0.56 ± 0.09% in control group, 0.53 ± 0.04% in control with HRS group, versus 7.02 ± 0.15% in SE group and 1.4 ± 0.13% in SE with HRS group (Fig. 6h). Furthermore, the proportions of $MLKL^+$-$NeuN^+$ cells within

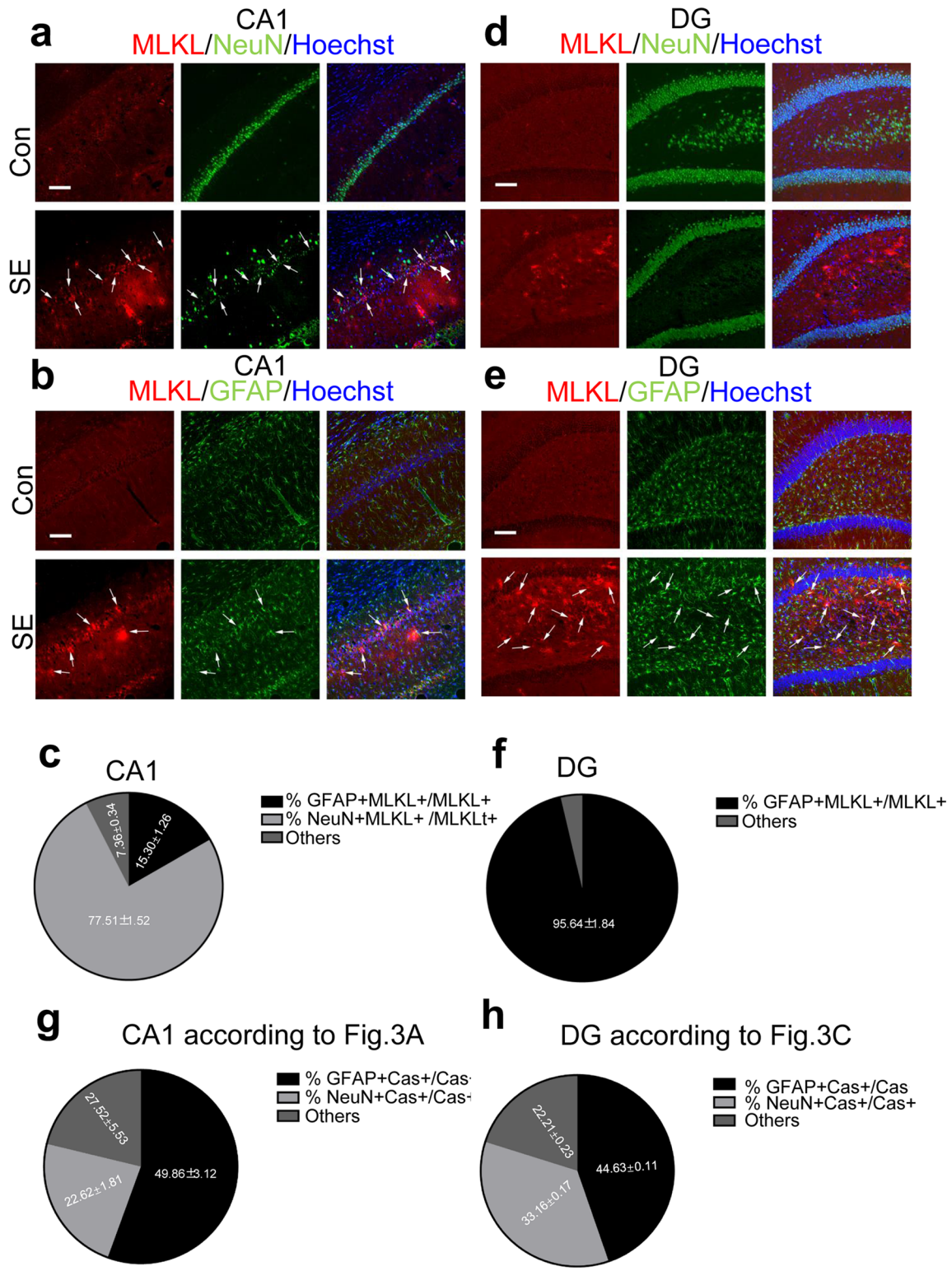

Fig. 5 Cell type analysis of cells undergoing necroptosis in hippocampus. Based on previous observation in Fig. 4, cells expressing MLKL in CA1 (**a**–**c**) and in hilus of DG (**d**–**f**) were further stained with cell type markers. **a**–**c** In CA1 area, cells expressing both MLKL and NeuN accounted for 77.51 ± 1.52% of total MLKL$^+$ cells, indicating that most MLKL-expressing cells in CA1 were neurons. Only 15.3 ± 1.26% of MLKL$^+$ cells also showed GFAP expression. **d**–**f** In hilus of DG, cells were also analyzed. 95.64 ± 1.84% of MLKL$^+$ cells were GFAP$^+$ astrocytes, and no NeuN$^+$ neurons were found in MLKL$^+$ cells in hilus of DG. **g**, **h** As a reference, the proportions of apoptotic neurons or astrocytes in total apoptotic cells in CA1 and in DG of SE rats were also calculated. Data were presented as mean ± SEM. Scale bar: 100 μm in **a**, **b**, **d**, and **e**

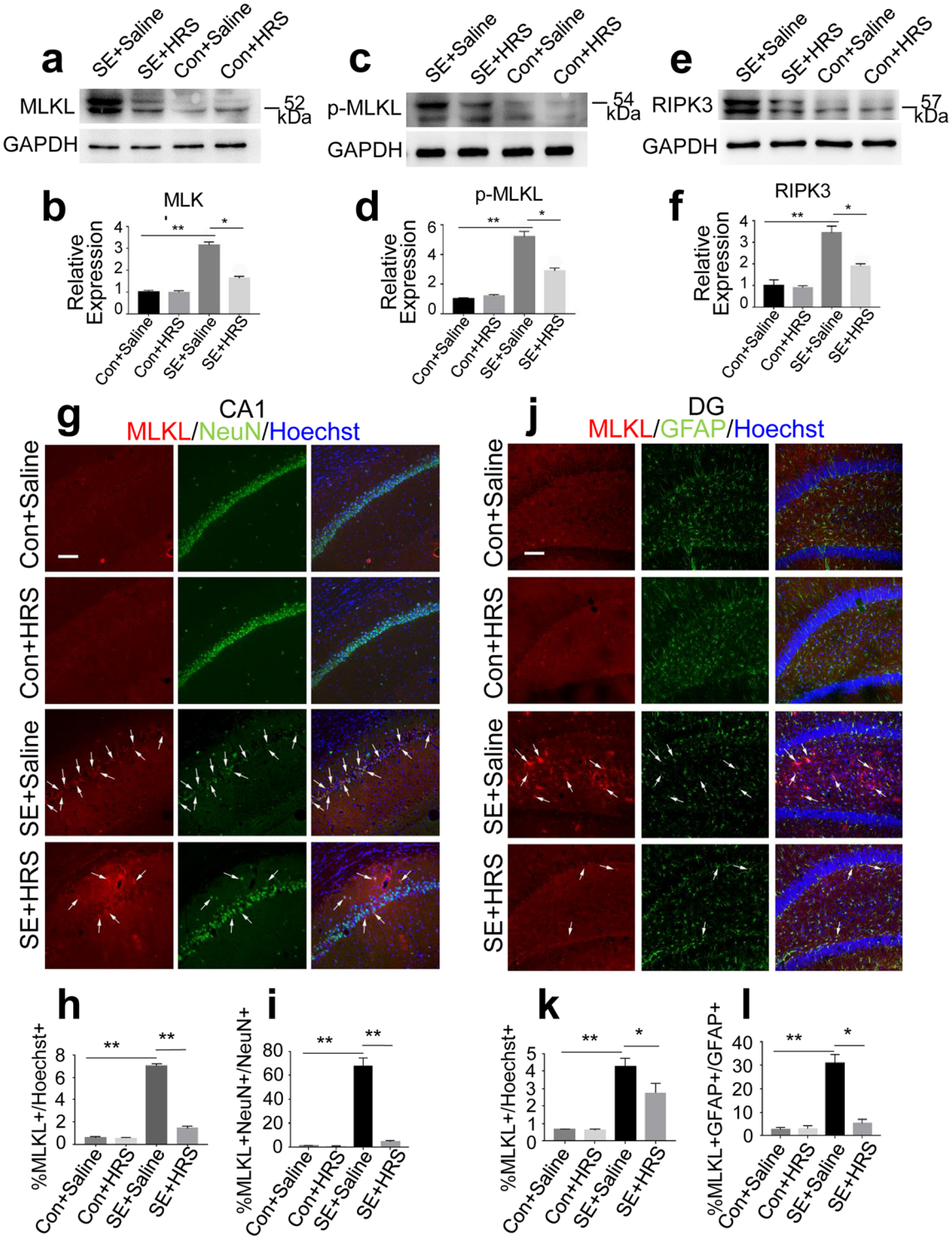

Fig. 6 Protective effects of HRS on necroptosis after SE. **a**–**f** The expressions of MLKL, p-MLKL, and RIP3 in CA1 of each group were tested by WB and the corresponding quantified results were analyzed and presented ($n=3$ in each group). **g**–**i** Immunofluorescence stainings of MLKL and NeuN were performed in CA1. Arrows in **g** indicated the cells expressing both MLKL and NeuN. The results of statistical analysis are shown in **h**, **i**. We analyzed the percentage of $MLKL^+$ cells in $Hoechst^+$ total cells within a field (**h**) and the percentage of cells expressing both NeuN and MLKL in $NeuN^+$ neurons (**i**). **j**–**l** Similarly, immunofluorescence stainings of MLKL and GFAP were performed in DG (**j**). And the statistical results were presented in **k** and **l**. Data were presented as mean ± SEM and n = 3 in all groups. * $P<0.05$; ** $P<0.01$. Scale bar: 100 μm in **g** and **j**

NeuN$^+$ neurons (Fig. 6i) were 0.9 ± 0.26%, 0.53 ± 0.23%, 67.36 ± 4.23%, and 4.46 ± 0.55% separately. These data showed that the expression of MLKL in SE hippocampus increased compared to control ones, and importantly, it decreased significantly after HRS treatment (Fig. 6h, i). Similarly, in hilus of DG (Fig. 6j–l), SE induced the elevation of MLKL expression within total cells (Fig. 6k) and also in GFAP$^+$ astrocytes (Fig. 6l), and hydrogen reduced this elevation from 4.25 ± 0.28 to 2.75 ± 0.32% (Fig. 6k) in total cell population and from 30.93 ± 3.79 to 5.17 ± 1.07% in GFAP$^+$ astrocytes (Fig. 6l). These results suggested that hydrogen had a protective effect on SE-induced cell necroptosis in hippocampus through protecting neurons in CA1 and astrocytes in hilus of DG.

The Inflammation was also Reduced in HRS-Treated Group

Necroptosis may induce inflammation. We, therefore, explored the inflammation response by Iba1 (ionized calcium binding adaptor molecule, a specific microglial marker) immunostaining. The staining in CA1 (Fig. 7a–c) and in hilus (Fig. 7d–f) sub-regions showed that in control group and HRS-treated control group the expressions of Iba1 signal were weak and the positive cells were few in number and small in size, but in SE group, both the number of Iba1$^+$ microglial cells (Fig. 7b, e) and the pixels of Iba1 signal (Fig. 7c, f) significantly increased. The morphology of Iba1$^+$ cells in SE group also changed with the size enlarged and the branches increased (bottom of Fig. 7a, d). More importantly, hydrogen application could revert these signs of microglial activation. In HRS-treated SE group, the number of Iba1$^+$

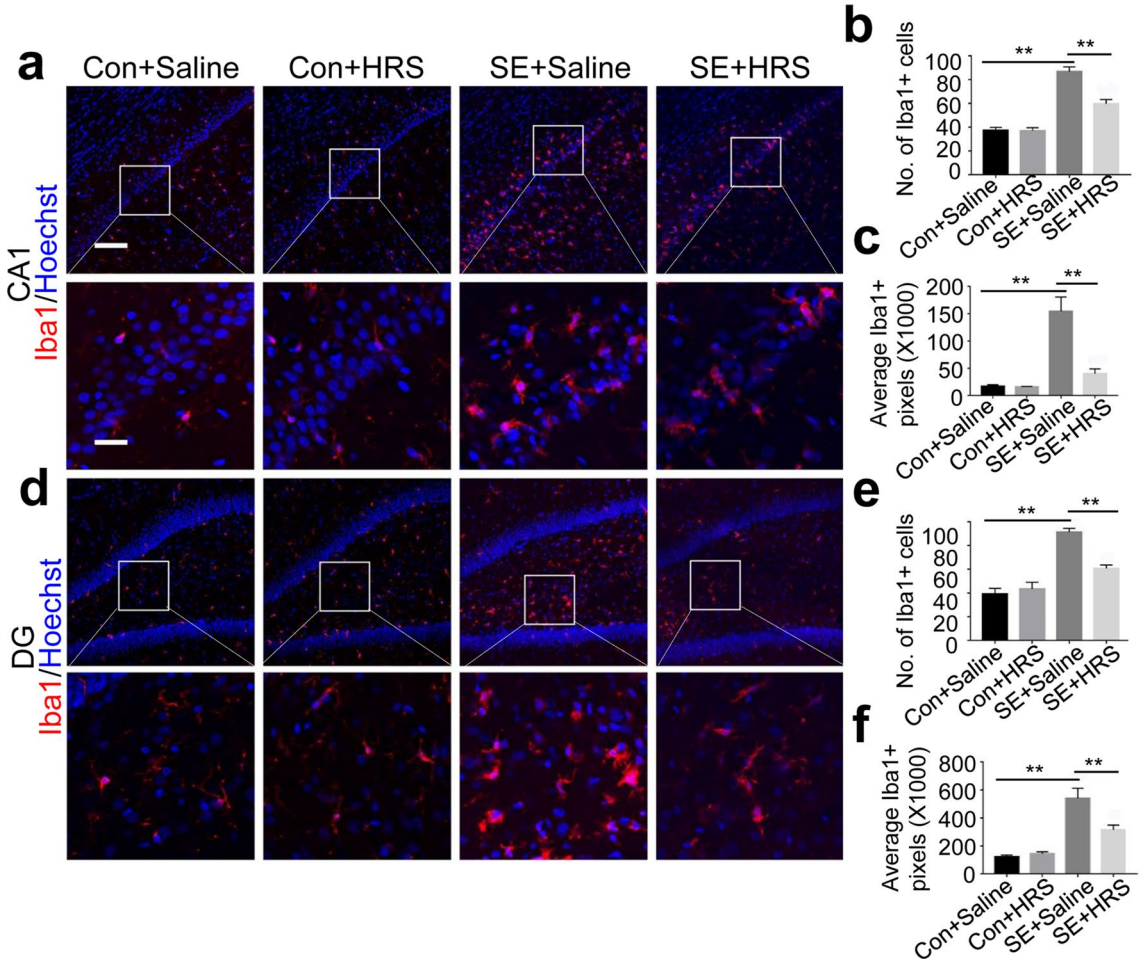

Fig. 7 The inflammation level in hippocampus. Immunofluorescence staining of Iba1 was performed to show the inflammation level in CA1 (**a**–**c**) and in hilus of DG (**d**–**f**). The parts enclosed by squares in top of **a** and **d** were enlarged in bottom of **a** and **d**. The statistical results included the number of Iba1$^+$ cells in one field (**b**, **e**) and the pixels of Iba1 expression (**c**, **f**) in order to reflect the changes of both numbers and forms of microglial cells. Data were presented as mean ± SEM and $n = 3$ in all groups. $^{**}P < 0.01$. Scale bar: 100 μm in top of **a** and **d**; 50 μm in bottom of **a** and **d**

microglia (Fig. 7b, e) and the pixels of Iba1 signal (Fig. 7c, f) decreased and the size of microglia shrank (bottom of Fig. 7a, d). These results suggested that hydrogen treatment could reduce the level of tissue inflammation induced by SE.

Discussion

In this study, we found that HRS improved the hippocampus-dependent cognition performance of rats after SE, including spatial learning and spatial memory abilities. We proved that SE led to necroptosis in hippocampus, which showed in specific sub-regions and cell types. The necroptosis was found in neurons of CA1 and in astrocytes of hilus of DG while apoptosis was uniformly distributed in both neurons and astrocytes of CA1, CA3, and DG. Hydrogen treatment alleviated both necroptosis and apoptosis, especially reduced the neuronal necroptosis in CA1. This utility of hydrogen eventually contributed to the recovery of hippocampus-related spatial learning and memory functions. Furthermore, SE-induced microglial inflammatory activation was relieved in the hippocampus of hydrogen-treated rats. This was at least partially due to the reduced necroptosis since necroptosis, unlike apoptosis, could induce inflammation (Pasparakis and Vandenabeele 2015; Newton and Manning 2016; Weinlich et al. 2017). Because inflammation may aggravate SE and SE-related comorbidities (Janigro et al. 2013; Vezzani et al. 2015; Auvin et al. 2016; van Vliet et al. 2018; Walker 2018; Wang and Chen 2018), this relieving of microglia activation should also contribute to the attenuation of cognitive impairments. While the mechanisms still need to be studied, our research demonstrated that hydrogen could prevent the SE-induced spatial learning and memory deficits through protecting the hippocampal neurons from necroptosis and apoptosis and reducing the subsequent inflammation levels.

The capability of hydrogen to prevent cognitive impairments was the focus of this research. First, SE impaired spatial learning and memory ability, and this was evidenced by the following results including the nearly unchanged escape latency to the platform as training progressed, the reduced amount of time spent searching the target quadrant, and the decreased frequency that rats entered into the target quadrant in the probe trial. Second, the administration of HRS attenuated these impairments of spatial learning ability and spatial memory ability. In HRS-treated SE rats, the latency to the platform became shorter during training days although it had not recovered to the level of control rats. This reduction during learning process emphasized on the spatial learning ability and suggested HRS could improve it. The time HRS-treated SE rats spent in the target quadrant returned to the comparable amount of time that control rats spent. And the frequency into the target quadrant also moderately increased by hydrogen. The above two parameters emphasized on the spatial memory ability and indicated the improvement of it by hydrogen. Thus, the administration of hydrogen allowed prevention of the cognitive comorbidities after SE, such as spatial learning and memory deficits. Therefore, hydrogen provides a potentially useful method for clinical treatment.

Cell death within hippocampus triggered by SE plays an important role in SE-related cognitive deficits. Li-Pilo-induced SE on rats is a good model because the extensive neuronal death occurs in CA1, CA3, and DG of hippocampal regions, a pattern similar to hippocampal sclerosis in human temporal lobe epilepsy (Sharma et al. 2007; Curia et al. 2008; Levesque et al. 2016). Previous studies indicated that neurons in these regions could undergo necrosis, apoptosis, and so on (Sloviter et al. 1996; Fujikawa et al. 1999; Bengzon et al. 2002; Li et al. 2013; Long et al. 2014; Shiha et al. 2015). There are many studies about necrosis and apoptosis in SE but less about necroptosis. For example, apoptosis was proved by positive TUNEL staining, increased expression of apoptotic protein, and activation of related pathways (Sloviter et al. 1996; Bengzon et al. 2002; Li et al. 2013; Long et al. 2014; Shiha et al. 2015). And some studies also proved the appearance of necrosis in hippocampus of experimental SE model (Sloviter et al. 1996; Fujikawa et al. 1999). Some data even further pointed out the different susceptibility to necrosis and apoptosis by cells in different parts of hippocampus (Sloviter et al. 1996). These accumulated lines of evidence showed that apoptotic and necrotic cell deaths contribute to brain damage in SE. A few research projects indicated the involvement of necroptosis in SE, but lack the direct evidence. In juvenile rats of 25 days old, MLKL was expressed in cells in the amygdala and piriform cortex after SE (Cai et al. 2017). But this experiment in juvenile rats could not indicate the situation in adult SE rats since the features of seizure-induced injury in immature brains were different from those in adult mature brains (Haut et al. 2004). Furthermore, in this experiment, necroptosis was only indicated by MLKL immunostaining. Another two studies showed that in the Li-Pilo-induced SE adult model, the expressions of the related proteins like MLKL would decrease after some drug treatments (Wang et al. 2017a, b). However, necroptosis in these two studies was also only indicated by MLKL immunostaining and the detailed situation of necroptosis was absent. For example, they did not show whether different sub-regions of hippocampus have different susceptibility to necroptosis.

In our research, we managed to answer these questions to provide more information. The expressions of necroptosis-related molecules such as MLKL, p-MLKL, and RIPK3 were proved to increase after SE by WB analysis first. The expression of MLKL was further proved by immunofluorescence staining to describe the in situ situation in hippocampus. And the observation by TEM strongly supports the occurrence of necroptosis. These data altogether

provided sufficient evidence to support the idea that cells in hippocampus would undergo necroptosis in adult SE rats and this would contribute to the destruction of hippocampal structure and function after SE. Our data also indicated the different susceptibility to necroptosis by cells in different sub-regions of hippocampus. Neurons in CA1 and astrocytes in hilus of DG were more vulnerable to necroptosis. Previous study showed that neurons in hilus of DG and in CA1 were more prone to necrosis and dentate granule cells were prone to apoptosis (Sloviter et al. 1996). Our data and these studies were consistent and all pointed to the opinion that cells in different parts of hippocampus have different susceptibility to different forms of death triggered by SE. Although the underlying mechanism still needs to be explored, this realization would be helpful for the development of different strategies for targeting different forms of death in SE. Our hydrogen treatment could ameliorate both necroptosis and apoptosis in hippocampus of SE rats, with the obvious effect on neuronal necroptosis in CA1 region. This amelioration would reduce the damage SE caused to the hippocampal structure and to hippocampus-dependent behaviors.

The inflammation induced by necroptosis was also preliminarily observed in this study. Mounting evidence has indicated that inflammation is a consequence as well as a facilitator of seizures (Vezzani et al. 2011) and plays a key role in ongoing seizures and their long-term brain function deficits independent of the causes of inflammation (Garcia-Morales et al. 2008; Janigro et al. 2013). Necroptosis, the newly discovered pathway of regulated necrosis, can trigger an immune response with the dying cell rupturing and releasing intracellular components (Pasparakis and Vandenabeele 2015; Newton and Manning 2016; Weinlich et al. 2017). Some studies even revealed the possibility that necroptosis is but one mechanism by which the related-kinases promote inflammation (Newton and Manning 2016). Since necroptosis was observed to be decreased by hydrogen in this study, we inferred that inflammation might also be reduced by hydrogen application, which could promote the affected cognitive ability ensuing in the brain. The results has confirmed this inference. The inflammation indicated by Iba1 immunostaining of microglial activation was increased after SE but decreased after hydrogen application, which indicated that hydrogen could alleviate the inflammation in SE. This alleviation was at least partially due to the decreased necroptosis. Although precise mechanisms remain to be elucidated, the beneficial effects of hydrogen on inflammation and thereafter on behaviors have been demonstrated in our study.

Altogether, hydrogen treatment protected hippocampal cells mainly by reducing neuronal and astrocytic necroptosis, but also including apoptosis in Li-Pilo-induced SE models. The reduced necroptosis may lead to reduced inflammation level in hippocampus. All these protection effects could improve the SE-impaired spatial learning and memory ability. Therefore, hydrogen has great potential to be a clinical treatment for SE-induced cognitive dysfunction.

Acknowledgements This work was supported by the National Natural Science Foundation (Grant Nos. 81771406, 81571262) and the Shaanxi Natural Science Foundation (Grant Nos. 2018KW-063, 2016SF-221).

Author Contributions WJ and FG designed the experiments; RJ, NJ, FY, ZL, and HZ performed the experiments of making SE model, immunofluorescence staining, and Western Blot analysis; RJ, ZL, and RL carried out Morris Water maze tests; RJ, YJ, JZ, and LW performed the statistical analysis; FG, RJ, SZ, ZZ, and WJ contributed to writing. All authors have read and approved the final manuscript.

Compliance with Ethical Standards

Conflict of interest The authors declare that they have no conflict of interest.

References

Auvin S, Cilio MR, Vezzani A (2016) Current understanding and neurobiology of epileptic encephalopathies. Neurobiol Dis 92:72–89. https://doi.org/10.1016/j.nbd.2016.03.007

Bengzon J, Mohapel P, Ekdahl CT et al (2002) Neuronal apoptosis after brief and prolonged seizures. Prog Brain Res 135:111–119. https://doi.org/10.1016/S0079-6123(02)35011-8

Betjemann JP, Lowenstein DH (2015) Status epilepticus in adults. Lancet Neurol 14:615–624. https://doi.org/10.1016/S1474-4422(15)00042-3

Cai J, Kang Z, Liu K et al (2009) Neuroprotective effects of hydrogen saline in neonatal hypoxia-ischemia rat model. Brain Res 1256:129–137. https://doi.org/10.1016/j.brainres.2008.11.048

Cai Q, Gan J, Luo R et al (2017) The role of necroptosis in status epilepticus-induced brain injury in juvenile rats. Epilepsy Behav 75:134–142. https://doi.org/10.1016/j.yebeh.2017.05.025

Curia G, Longo D, Biagini G et al (2008) The pilocarpine model of temporal lobe epilepsy. J Neurosci Methods 172:143–157. https://doi.org/10.1016/j.jneumeth.2008.04.019

Fan H, Zhang K, Shan L et al (2016) Reactive astrocytes undergo M1 microglia/macrohpages-induced necroptosis in spinal cord injury. Mol Neurodegener 11:14. https://doi.org/10.1186/s13024-016-0081-8

Fujikawa DG, Shinmei SS, Cai B (1999) Lithium-pilocarpine-induced status epilepticus produces necrotic neurons with internucleosomal DNA fragmentation in adult rats. Eur J Neurosci 11:1605–1614

Garcia-Morales I, de la Pena MP, Kanner AM (2008) Psychiatric comorbidities in epilepsy: identification and treatment. Neurologist 14:S15–S25. https://doi.org/10.1097/01.nrl.0000340788.07672.51

Gokalp N, Basaklar AC, Sonmez K et al (2017) Protective effect of hydrogen rich saline solution on experimental ovarian ischemia reperfusion model in rats. J Pediatr Surg 52:492–497. https://doi.org/10.1016/j.jpedsurg.2016.10.006

Haut SR, Veliskova J, Moshe SL (2004) Susceptibility of immature and adult brains to seizure effects. Lancet Neurol 3:608–617. https://doi.org/10.1016/S1474-4422(04)00881-6

Haut SR, Seinfeld S, Pellock J (2016) Benzodiazepine use in seizure emergencies: a systematic review. Epilepsy Behav 63:109–117. https://doi.org/10.1016/j.yebeh.2016.07.018

Iida A, Nosaka N, Yumoto T et al (2016) The clinical application of hydrogen as a medical treatment. Acta Med Okayama 70:331–337. https://doi.org/10.18926/AMO/54590

Janigro D, Iffland PN, Marchi N et al (2013) A role for inflammation in status epilepticus is revealed by a review of current therapeutic approaches. Epilepsia 54(Suppl 6):30–32. https://doi.org/10.1111/epi.12271

Levesque M, Avoli M, Bernard C (2016) Animal models of temporal lobe epilepsy following systemic chemoconvulsant administration. J Neurosci Methods 260:45–52. https://doi.org/10.1016/j.jneumeth.2015.03.009

Li LY, Li JL, Zhang HM et al (2013) TGF beta1 treatment reduces hippocampal damage, spontaneous recurrent seizures, and learning memory deficits in pilocarpine-treated rats. J Mol Neurosci 50:109–123. https://doi.org/10.1007/s12031-012-9879-1

Long Q, Fan C, Kai W et al (2014) Hypoxia inducible factor-1alpha expression is associated with hippocampal apoptosis during epileptogenesis. Brain Res 1590:20–30. https://doi.org/10.1016/j.brainres.2014.09.028

Newton K, Manning G (2016) Necroptosis and inflammation. Annu Rev Biochem 85:743–763. https://doi.org/10.1146/annurev-biochem-060815-014830

Ohsawa I, Ishikawa M, Takahashi K et al (2007) Hydrogen acts as a therapeutic antioxidant by selectively reducing cytotoxic oxygen radicals. Nat Med 13:688–694. https://doi.org/10.1038/nm1577

Ohta S (2014) Molecular hydrogen as a preventive and therapeutic medical gas: initiation, development and potential of hydrogen medicine. Pharmacol Ther 144:1–11. https://doi.org/10.1016/j.pharmthera.2014.04.006

Okamoto A, Kohama K, Aoyama-Ishikawa M et al (2016) Intraperitoneally administered, hydrogen-rich physiologic solution protects against postoperative ileus and is associated with reduced nitric oxide production. Surgery 160:623–631. https://doi.org/10.1016/j.surg.2016.05.026

Pasparakis M, Vandenabeele P (2015) Necroptosis and its role in inflammation. Nature 517:311–320. https://doi.org/10.1038/nature14191

Pearson JN, Rowley S, Liang LP et al (2015) Reactive oxygen species mediate cognitive deficits in experimental temporal lobe epilepsy. Neurobiol Dis 82:289–297. https://doi.org/10.1016/j.nbd.2015.07.005

Schauwecker PE (2012) Strain differences in seizure-induced cell death following pilocarpine-induced status epilepticus. Neurobiol Dis 45:297–304. https://doi.org/10.1016/j.nbd.2011.08.013

Seinfeld S, Goodkin HP, Shinnar S (2016) Status epilepticus. Cold Spring Harb Perspect Med 6:a22830. https://doi.org/10.1101/cshperspect.a022830

Shao A, Wu H, Hong Y et al (2016) Hydrogen-rich saline attenuated subarachnoid hemorrhage-induced early brain injury in rats by suppressing inflammatory Response: possible involvement of NF-kappaB pathway and NLRP3 inflammasome. Mol Neurobiol 53:3462–3476. https://doi.org/10.1007/s12035-015-9242-y

Sharma AK, Reams RY, Jordan WH et al (2007) Mesial temporal lobe epilepsy: pathogenesis, induced rodent models and lesions. Toxicol Pathol 35:984–999. https://doi.org/10.1080/01926230701748305

Shiha AA, de Cristobal J, Delgado M et al (2015) Subacute administration of fluoxetine prevents short-term brain hypometabolism and reduces brain damage markers induced by the lithium-pilocarpine model of epilepsy in rats. Brain Res Bull 111:36–47. https://doi.org/10.1016/j.brainresbull.2014.12.009

Sloviter RS, Dean E, Sollas AL et al (1996) Apoptosis and necrosis induced in different hippocampal neuron populations by repetitive perforant path stimulation in the rat. J Comp Neurol 366:516–533. https://doi.org/10.1002/(SICI)1096-9861(19960311)366:3%3c516:AID-CNE10%3e3.0.CO;2-N

Sun Q, Cai J, Zhou J et al (2011) Hydrogen-rich saline reduces delayed neurologic sequelae in experimental carbon monoxide toxicity. Crit Care Med 39:765–769. https://doi.org/10.1097/CCM.0b013e318206bf44

Trinka E, Kalviainen R (2017) 25 years of advances in the definition, classification and treatment of status epilepticus. Seizure 44:65–73. https://doi.org/10.1016/j.seizure.2016.11.001

Trinka E, Hofler J, Leitinger M et al (2015) Pharmacotherapy for status epilepticus. Drugs 75:1499–1521. https://doi.org/10.1007/s40265-015-0454-2

Trinka E, Brigo F, Shorvon S (2016) Recent advances in status epilepticus. Curr Opin Neurol 29:189–198. https://doi.org/10.1097/WCO.0000000000000307

van Vliet EA, Aronica E, Vezzani A et al (2018) Review: neuroinflammatory pathways as treatment targets and biomarker candidates in epilepsy: emerging evidence from preclinical and clinical studies. Neuropathol Appl Neurobiol 44:91–111. https://doi.org/10.1111/nan.12444

Vezzani A, French J, Bartfai T et al (2011) The role of inflammation in epilepsy. Nat Rev Neurol 7:31–40. https://doi.org/10.1038/nrneurol.2010.178

Vezzani A, Dingledine R, Rossetti AO (2015) Immunity and inflammation in status epilepticus and its sequelae: possibilities for therapeutic application. Expert Rev Neurother 15:1081–1092. https://doi.org/10.1586/14737175.2015.1079130

Walker MC (2018) Pathophysiology of status epilepticus. Neurosci Lett 667:84–91. https://doi.org/10.1016/j.neulet.2016.12.044

Wang M, Chen Y (2018) Inflammation: a network in the pathogenesis of status epilepticus. Front Mol Neurosci 11:341. https://doi.org/10.3389/fnmol.2018.00341

Wang W, Tian L, Li Y et al (2013) Effects of hydrogen-rich saline on rats with acute carbon monoxide poisoning. J Emerg Med 44:107–115. https://doi.org/10.1016/j.jemermed.2012.01.065

Wang J, Li Y, Huang WH et al (2017a) The protective effect of Aucubin from *Eucommia ulmoides* against status epilepticus by inducing autophagy and inhibiting necroptosis. Am J Chin Med 45:557–573. https://doi.org/10.1142/S0192415X17500331

Wang J, Liu Y, Li XH et al (2017b) Curcumin protects neuronal cells against status-epilepticus-induced hippocampal damage through induction of autophagy and inhibition of necroptosis. Can J Physiol Pharmacol 95:501–509. https://doi.org/10.1139/cjpp-2016-0154

Weinlich R, Oberst A, Beere HM et al (2017) Necroptosis in development, inflammation and disease. Nat Rev Mol Cell Biol 18:127–136. https://doi.org/10.1038/nrm.2016.149

Yang J, Zhao Y, Zhang L et al (2018) RIPK3/MLKL-mediated neuronal necroptosis modulates the M1/M2 polarization of microglia/macrophages in the ischemic cortex. Cereb Cortex 28:2622–2635. https://doi.org/10.1093/cercor/bhy089

Zhang S, Tang MB, Luo HY et al (2017) Necroptosis in neurodegenerative diseases: a potential therapeutic target. Cell Death Dis 8:e2905. https://doi.org/10.1038/cddis.2017.286